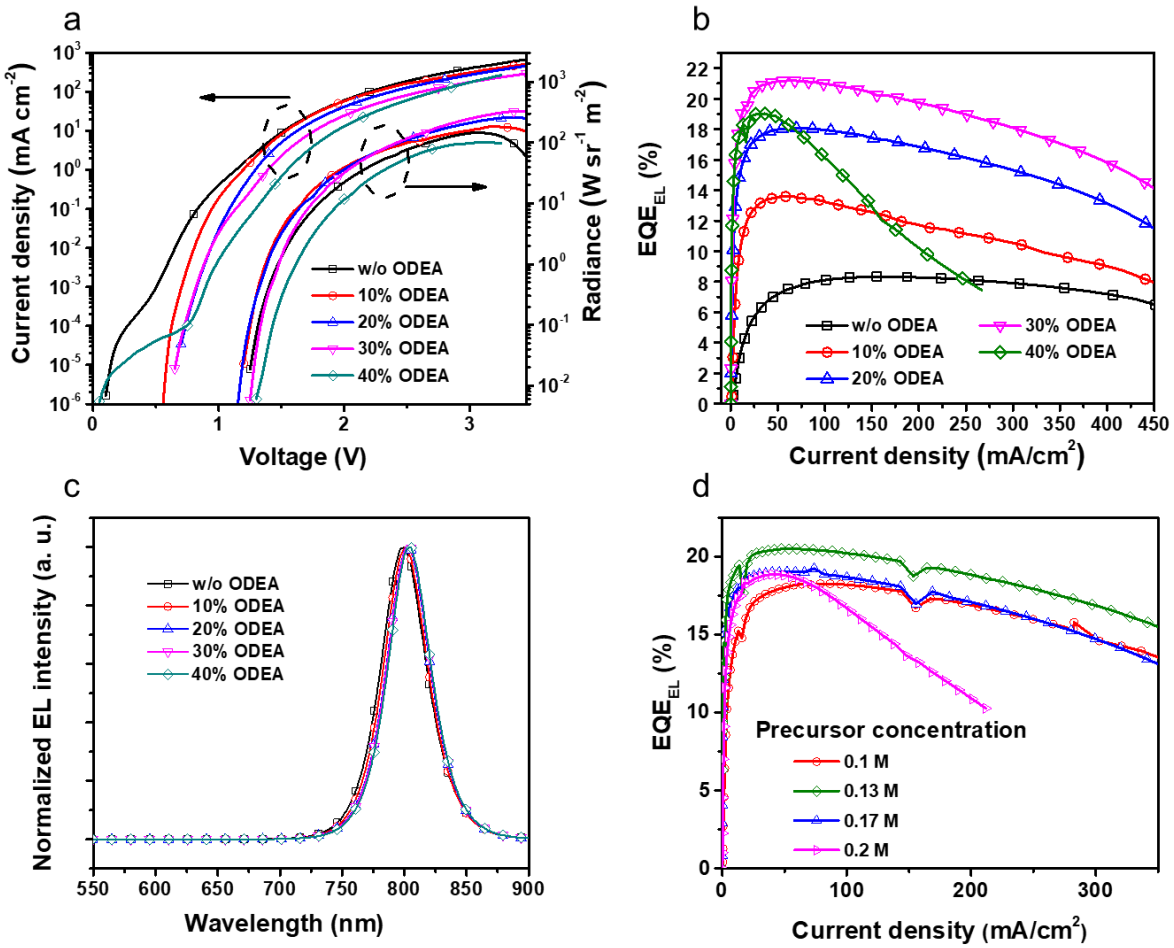

Supplementary Figure 1 Electroluminescence performance of the perovskite LED. a, Current density and radiance versus voltage curves of perovskite LEDs based on perovskite films with different amount of ODEA additives. **b,** External quantum efficiency (EQE) versus drive current density of perovskite LEDs based on perovskite films with different amount of ODEA additives. **c,** Electroluminescence spectra of perovskite LEDs based on perovskite films with different amount of ODEA additives. **d,** External quantum efficiency (EQE) versus drive current density of perovskite LEDs based on perovskite films made from precursors with different concentrations.

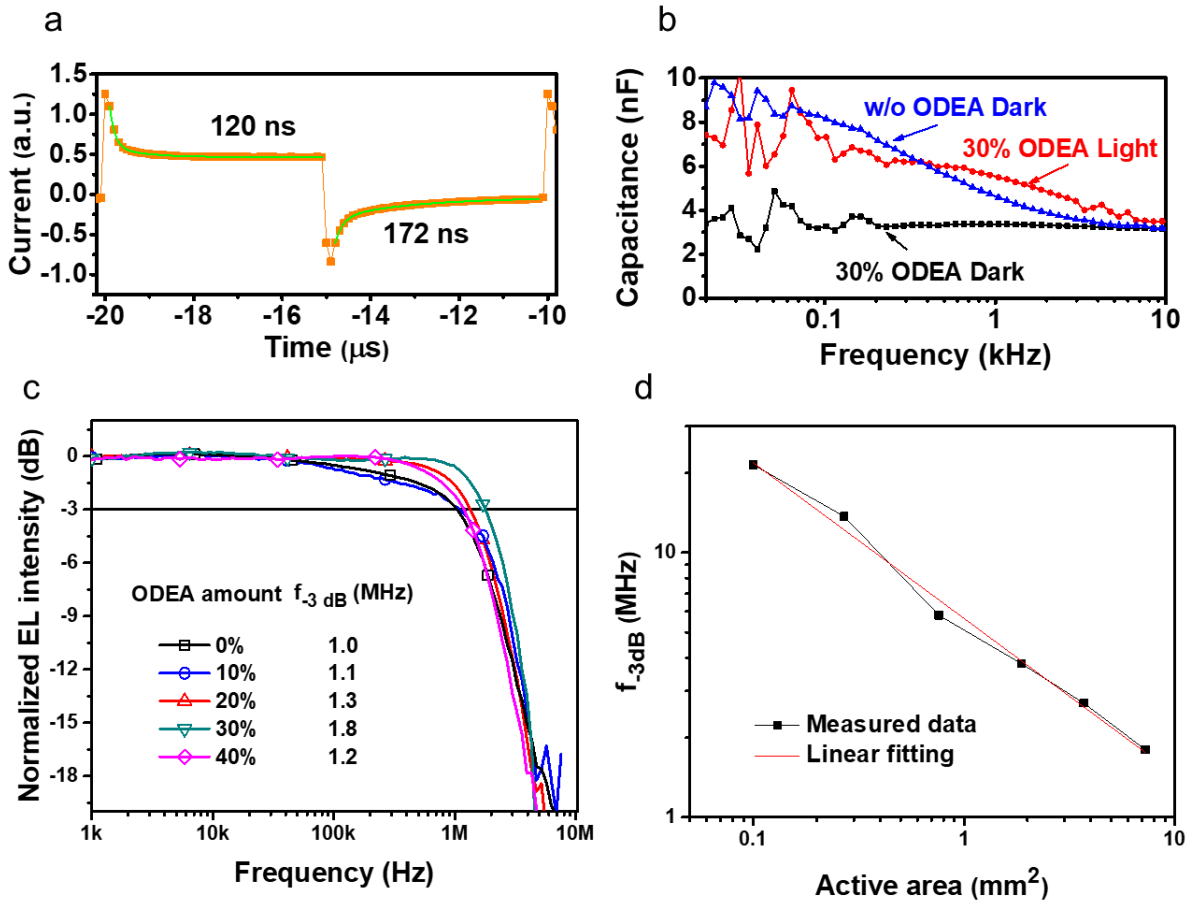

Supplementary Figure 2 Response speed characterizations of perovskite diodes when working as LEDs. a, Fitting curves of the LED transient current with exponential function. **b,** The measured capacitance spectra of the perovskite LEDs under dark and illumination of 450 nm monochrome light with power of ~1 μW. **c.** Frequency response curves of perovskite LEDs based on perovskite films with different amount of OEDA additives. **d,** Cut-off frequencies of perovskite LEDs with different device areas.

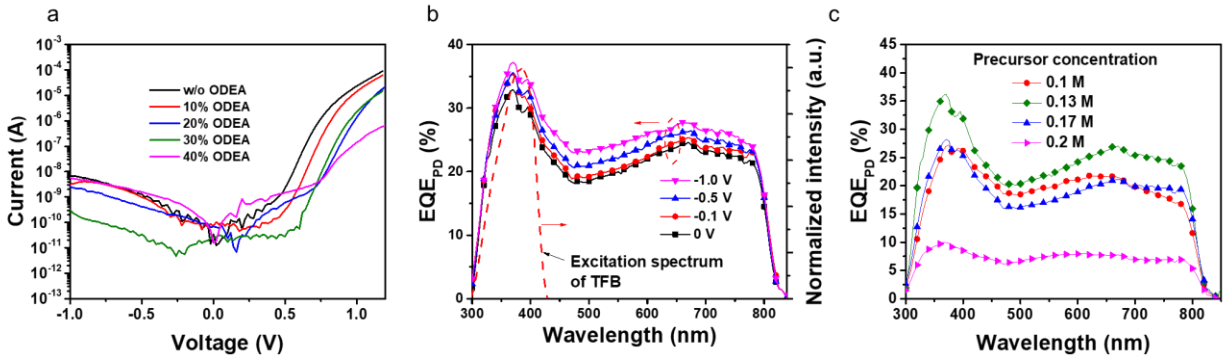

Supplementary Figure 3 Performance characterizations of perovskite photodetectors. a, Dark current vs voltage curves of perovskite photodetectors based on perovskite films with different amount of ODEA additives. **b,** External quantum efficiency (EQE) spectra of the perovskite photodetector under different biases as well as the excitation spectrum of TFB. **c,** EQE spectra of the perovskite photodetectors fabricated from perovskite precursors with different concentrations.

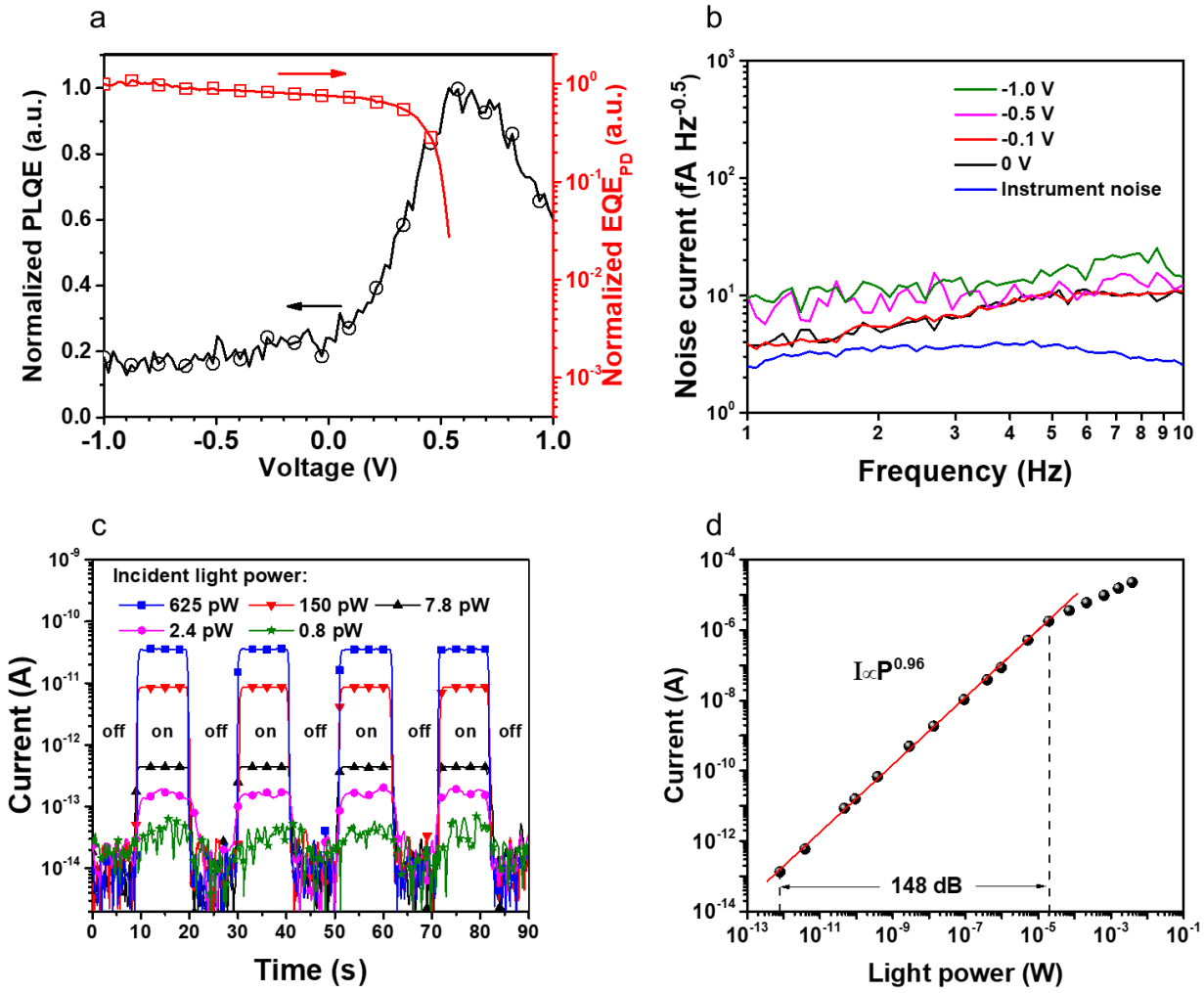

Supplementary Figure 4. **Performance characterizations of perovskite photodetectors. a,** Simultaneously measured photoluminescence quantum efficiency (PLQE) and photo-to-current conversion EQE of the perovskite diode. **b,** Noise current characteristics of the perovskite photodetector under different reverse biases as well as the noise current flow of the instrument. **c,** The current characteristics of the perovskite photodetector under illumination from an alternating on/off laser with different incident light power, indicating that the photodetector is sensitive to weak light of 0.8 pW. **d,** Linear dynamic range characteristic of the perovskite photodetector.

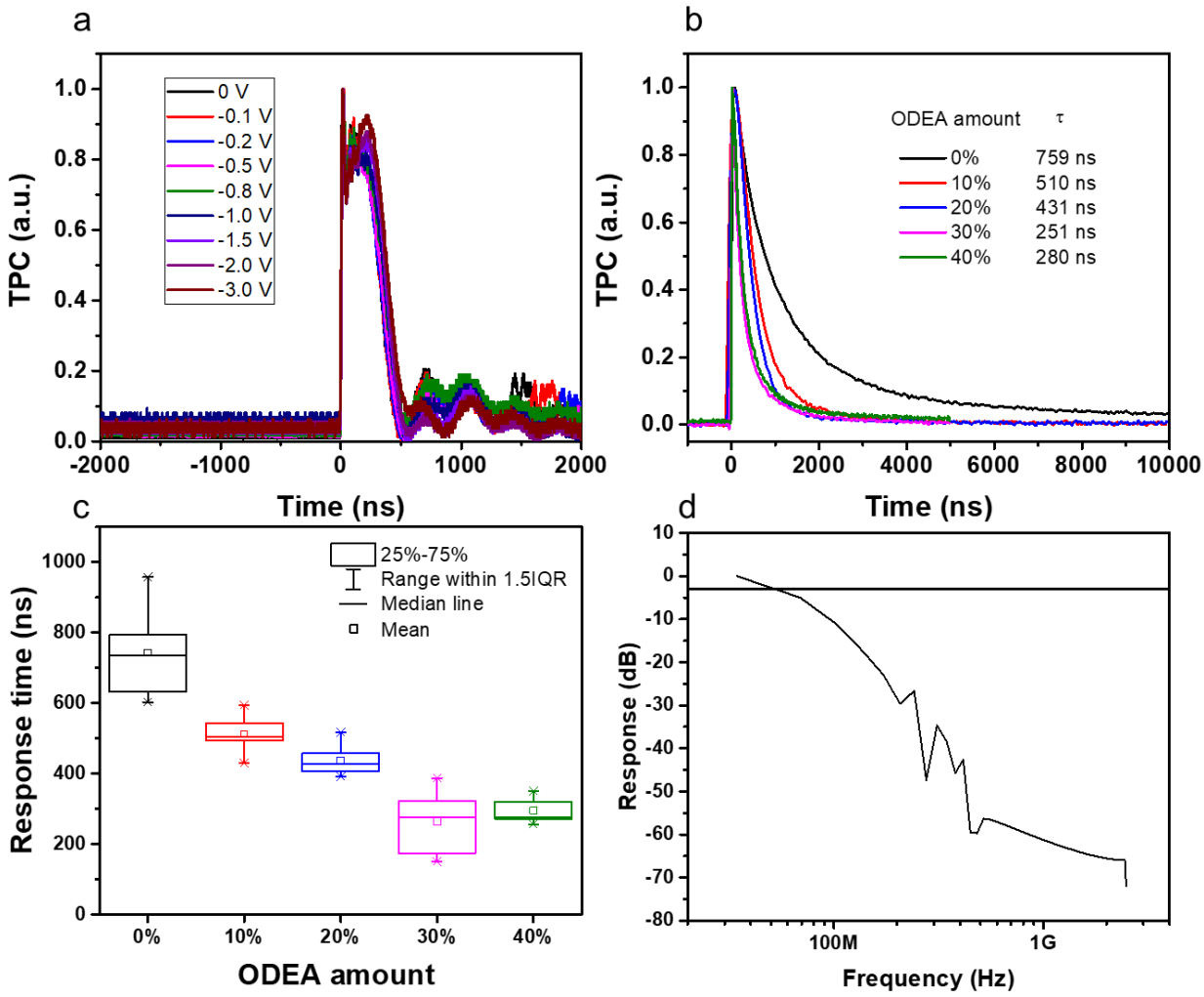

Supplementary Figure 5 Response speed of perovskite photodetectors. a, Transient photocurrent (TPC) of a perovskite photodetector under different bias voltages. **b,** TPC of perovskite photodetectors based on perovskite films with different amount of ODEA additives. **c,** Statistic box chart of the response time of perovskite photodetectors based on perovskite films with different amount of ODEA additives. The statistics is based on 6 different devices. **d.** Frequency response of the perovskite photodetector with the device area of 0.1 mm^2 obtained from the TPC curve by fast Fourier transform (FFT).

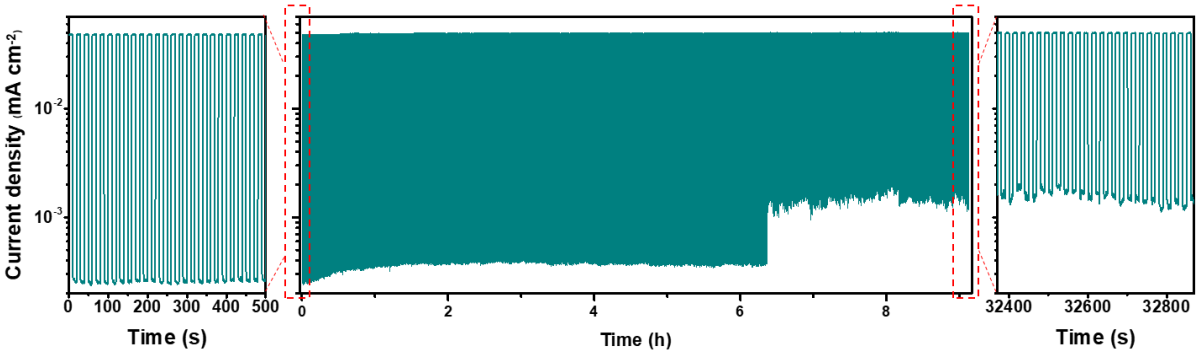

Supplementary Figure 6 Photo- and dark- current of the perovskite photodetector based on perovskite films without additives.

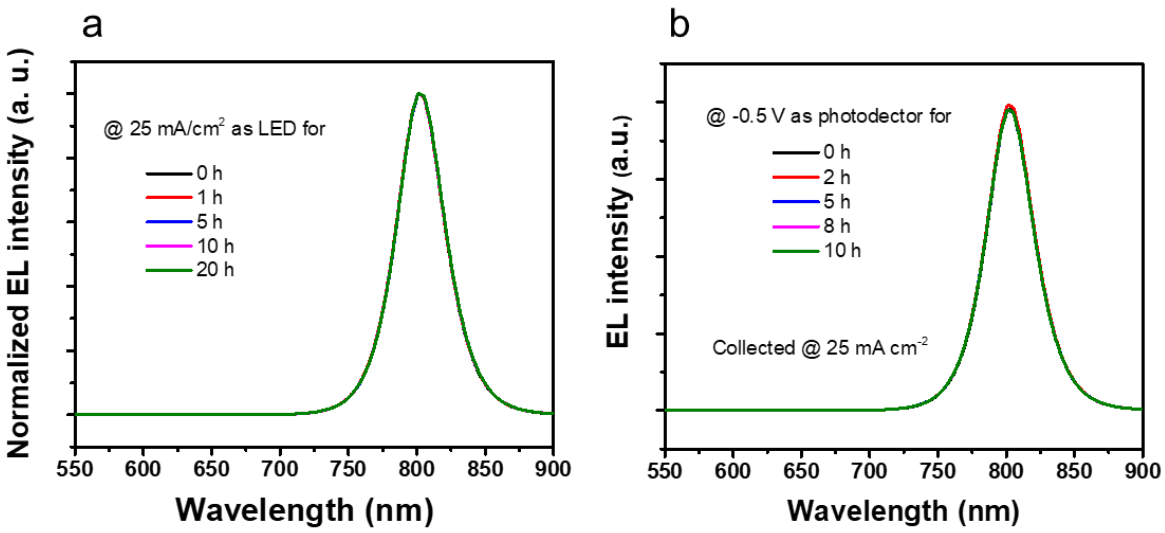

Supplementary Figure 7 EL spectrum stability of the diode after working as a light emitting (a) and detecting (b) device for a period of time.

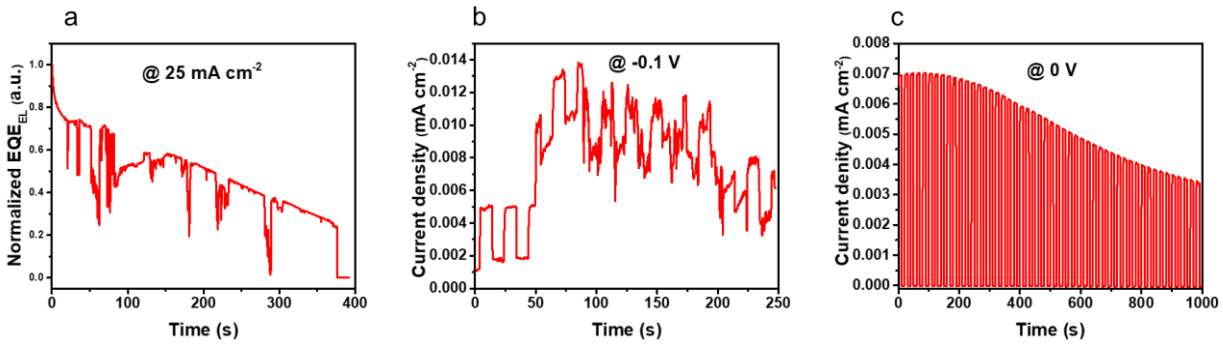

Supplementary Figure 8 The performance development of our devices measured under ambient conditions. a, Work as an LED at a current density of 25 mA cm^{-2}. **b,** Work as a photodetector at -0.1 V bias. **c,** Work as a photodetector at 0 bias. During the measurement, the relative humidity was ~37% and the temperature was ~18 °C.

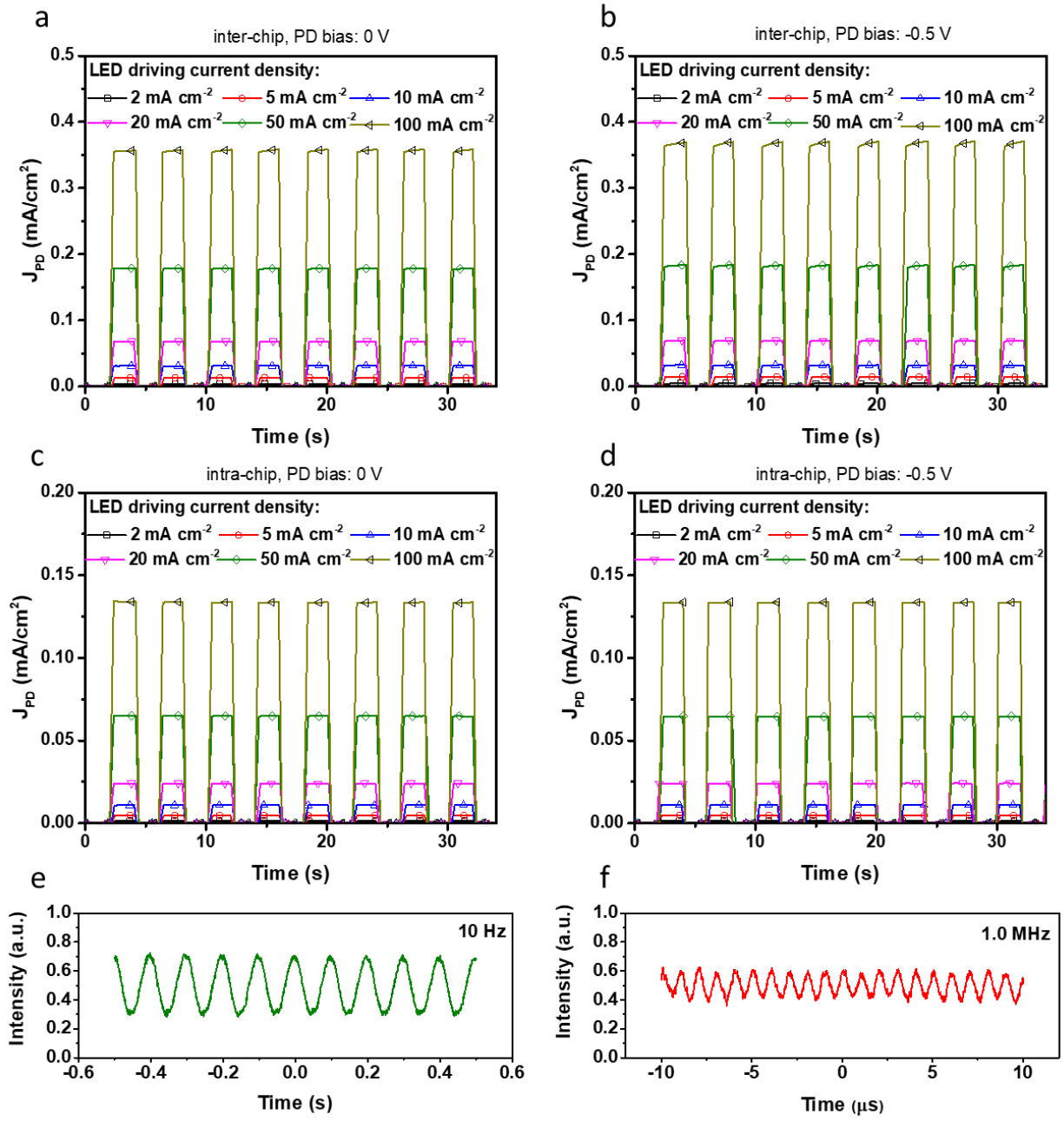

Supplementary Figure 9 Current transfer characterizations of dual-functional perovskite diodes. a, b, Current density of a perovskite photodetector under 0 V (a) and -0.5 V (b) bias voltages responding to the light emitted from an inter-chip perovskite LED under different drive current densities. **c, d,** Current density of a perovskite photodetector under 0 V (c) and -0.5 V (d) bias voltages responding to the light emitted from an intra-chip perovskite LED under different drive current densities. **e, f,** Response of the perovskite photodetector to the perovskite LED under modulation frequencies of 10 Hz (e) and 1 MHz (f).

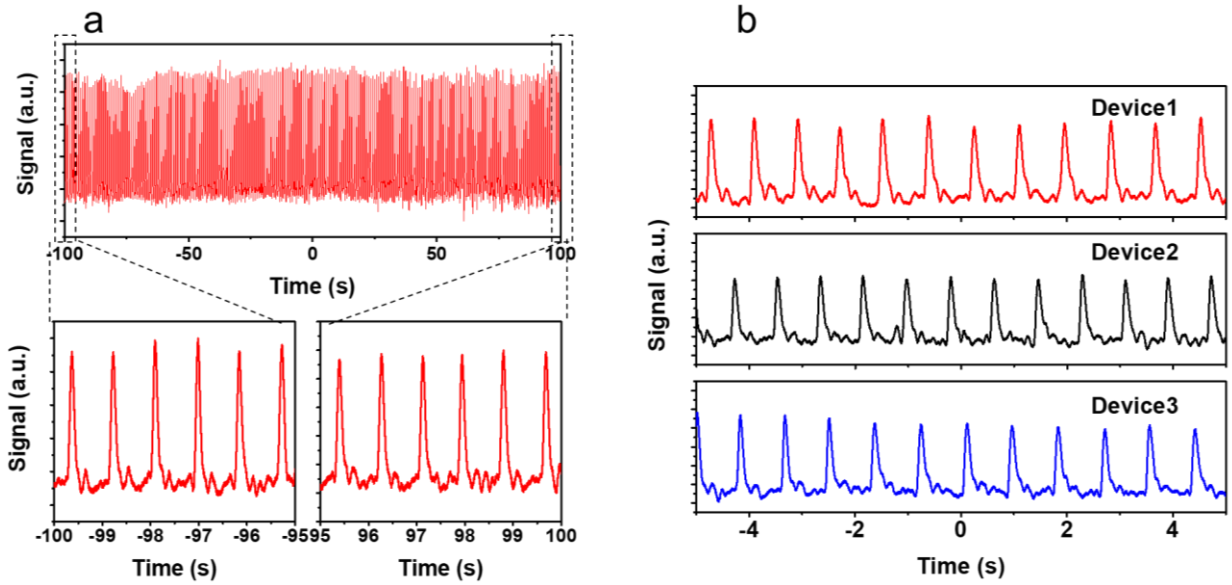

Supplementary Figure 10 Heart pulse waveforms collected using perovskite dual functional devices as the light source and detector. a, Waveforms collected during a period of 200 s. **b,** Waveforms monitored by three different perovskite devices.

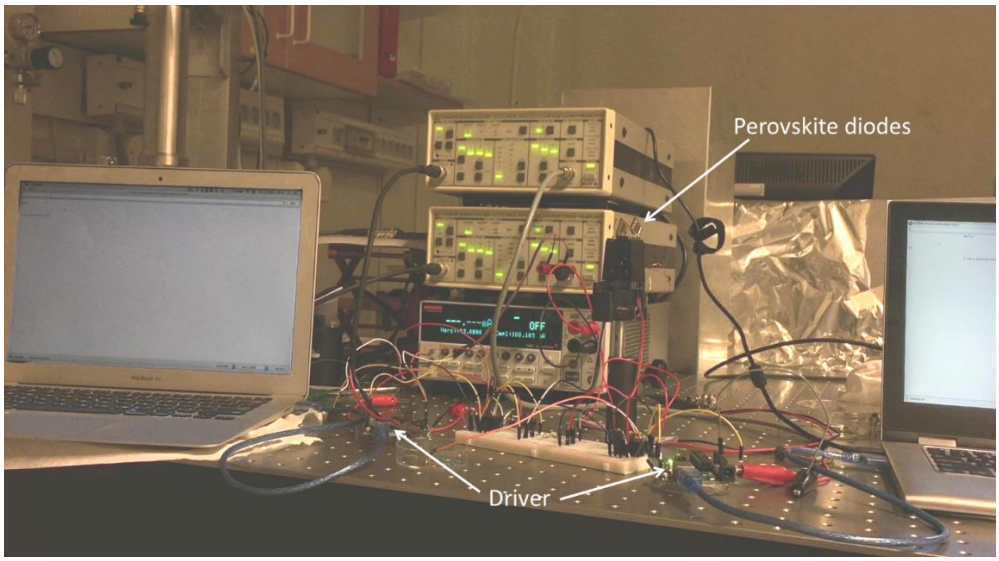

Supplementary Figure 11 The photograph of the bidirectional optical communication system using dual-functional perovskite diodes simultaneously as the transmitter and receiver.

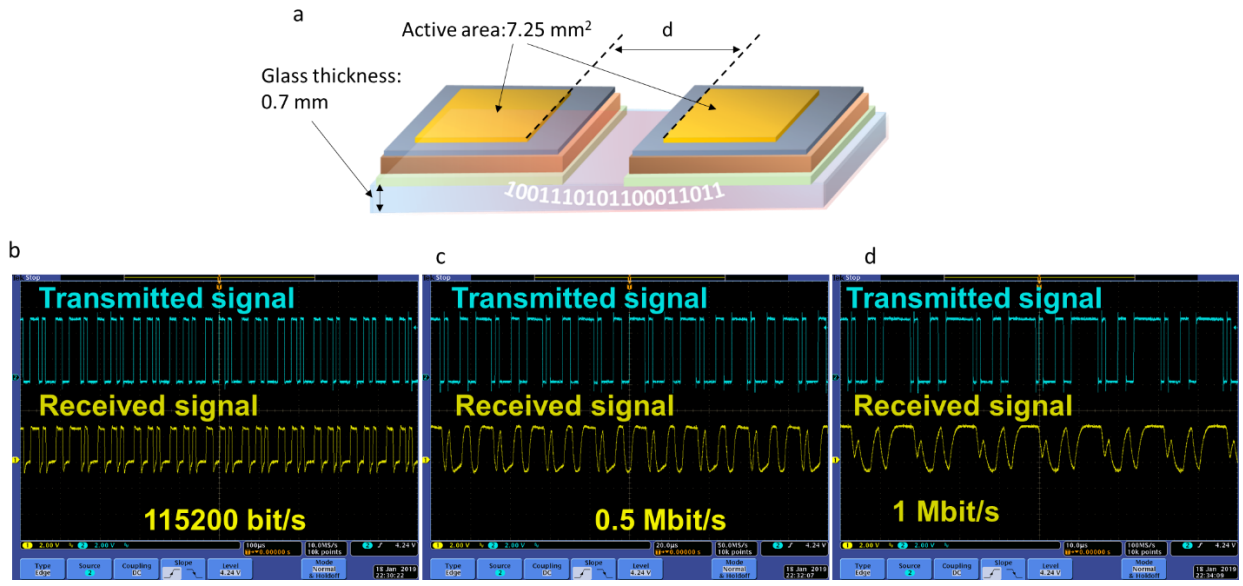

Supplementary Figure 12 Optical communication between two intra-chip dual-functional perovskite diodes. a, Dimension of the intra-chip dual-functional perovskite diodes. The distance d=1 mm in the intra-chip communication demonstration system. **b, c, d,** Waveforms of transmitted and received digital signals between these two dual-functional perovskite diodes at different bit rates.

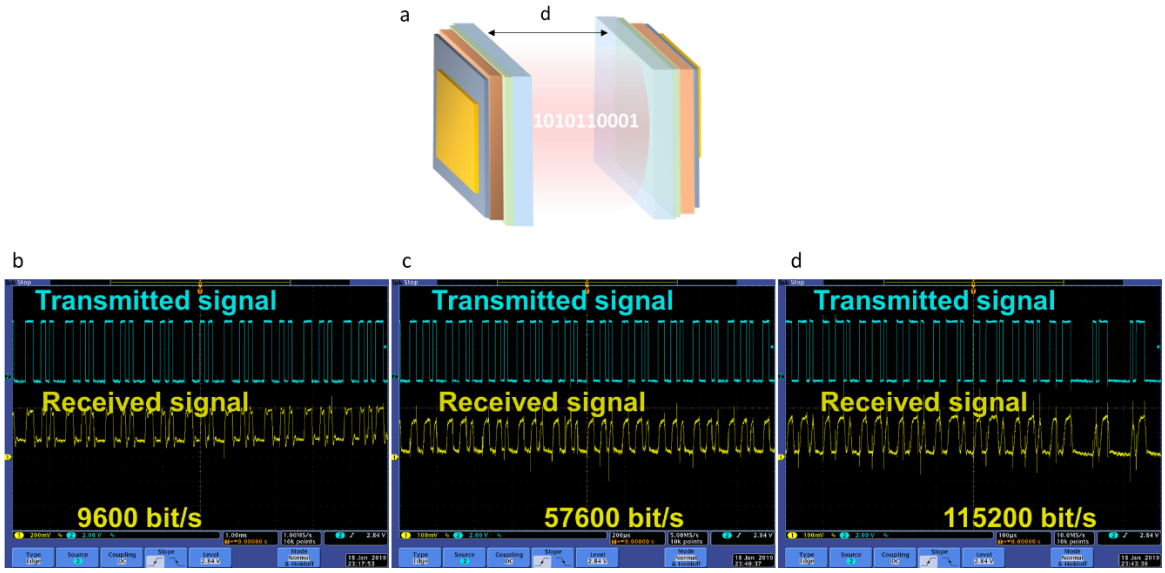

Supplementary Figure 13 Optical communication between two inter-chip dual-functional perovskite diodes. a, Dimension of the inter-chip dual-functional perovskite diodes. The distance d=13 mm in the inter-chip communication demonstration system. **b, c, d,** Waveforms of transmitted and received digital signals between these two dual-functional perovskite diodes at different bit rates.

Supplementary Note 1

For a photodiode, the response speed is mainly limited by two factors: the resistance-capacitance (RC) time constant induced by the resistance and parasitic capacitance, and the transit time (t_{tr}).[1,2]

$$f_{-3dB}^{-2} = \left(\frac{3.5}{2\pi t_{tr}}\right)^{-2} + \left(\frac{1}{2\pi RC}\right)^{-2} \quad \text{(S1)}$$

where f_{-3dB} is the 3-dB cutoff frequency. The RC constant can be effectively reduced by reducing the device area. Based on the capacitance measurement of our devices, the capacitance of the device with a small area of 0.01 mm^2 can be estimated to be ~ 4 pF. For a resistance of 50 Ω, we can obtain a RC constant of 0.2 ns, corresponding to a RC constant limited cutoff frequency of ~796 MHz.

The transit time for a diode can be expressed as[3]

$$t_{tr} = \frac{W_D}{\mu E} \quad \text{(S2)}$$

where W_D is the thickness of the depletion region, μ is the carrier mobility of the semiconductor, E is the electrical field intensity in the depletion region. In our device, the semiconductor layers can be considered as completely depleted layer due to the very small thickness and low free carrier concentration. So, we can use the thickness of the semiconductor to replace the thickness of the depletion region in function S2.

$$t_{tr} = \frac{d^2}{\mu V} \quad \text{(S3)}$$

where d is the thickness of the semiconductor, V is the sum of the applied reverse bias and the build-in voltage. For our device, considering the thickness and mobility difference, the transit time should be mainly determined by the transit time of the TFB layer. With the mobility (0.01 cm^{-2} V^{-1} s^{-1}, Ref 4) and the thickness (~40 nm) of TFB and the build-in voltage (~1.5 V), we can estimate the transit time of our device under 0 and -0.5 V bias as 1.1 and 0.8 ns, corresponding to transit time limited cutoff frequency of 525 and 697 MHz. When considering both RC constant and transit time, we can obtain the cutoff frequency of 438 and 524 MHz for 0 and -0.5 V biased device (device area: 0.01 mm^2), respectively.

From Functions S1 and S2 we can see that the response speed can be further improved by further decreasing the device area and increasing the reverse bias. But too small device area will lead to low signal-to-noise ratio, and high reverse bias is significantly harmful to the stability of perovskite devices. Other approaches to improving the response speed are to decrease the capacitance by increasing the junction thickness and to decrease the transit time by using high mobility materials to. For example, if the carrier mobility of the charge transport materials is 0.1 cm^{-2} V^{-1} s^{-1} and the thickness is 80 nm, then the capacitance will be reduced to ~2 pF for a device with area of 0.01 mm^2 (we assume the same dielectric constant). This corresponds to a RC time constant of 0.1 ns and a RC-constant-limited cutoff frequency of 1.6 GHz. According to Function S3, we can obtain a transit time of 0.32 ns, corresponding to a transit-time-limited cutoff frequency of 1.7 GHz.

For a light-emitting diode, in addition to the above electric-transport limiting factors, the emission decay time should be considered. If the device speed is limited by the emission decay time, a shorter emission decay time is necessary in order to obtain faster speed. For perovskite

devices with emission decay time of about 7 ns, the cutoff frequency has been experimentally demonstrated to be 491 MHz, and the device is capable in data transmission in a rate of ~2 Gbit/s when only the emission decay time is considered[5].

Supplementary Reference

1. Armin, A. *et al.* Thick junction broadband organic photodiodes. *Laser Photonics Rev.* **8,** 924–932 (2014).

2. Arquer, F. P. G., Armin, A., Meredith, P. & Sargent, E. H. Solution-processed semiconductors for next-generation photodetectors. *Nat. Rev. Mater,* **2**, 16100 (2017).

3. Clifford, J. P. *et al*. Fast, sensitive and spectrally tuneable colloidal-quantum-dot photodetectors. *Nat. Nanotech.* **4**, 40–44 (2009).

4. Fong, H.H., Papadimitratos, A. & Malliaras, G.G. Nondispersive hole transport in a polyfluorene copolymer with a mobility of $0.01 cm^2 V^{-1} s^{-1}$. *Appl. Phys. Lett*, **89**, 172116 (2006).

5. Dursun, I. *et al.* Perovskite Nanocrystals as a Color Converter for Visible Light Communication, *ACS Photonics*, **3**, 1150 (2016).